ORIGINAL PAPER

Accelerated pre-senile systemic amyloidosis in PACAP knockout mice – a protective role of PACAP in age-related degenerative processes

Dora Reglodi[1], Adel Jungling[1], Rémi Longuespée[2], Joerg Kriegsmann[3,4], Rita Casadonte[4], Mark Kriegsmann[2] ID, Tamas Juhasz[5], Sebastian Bardosi[3], Andrea Tamas[1], Balazs Daniel Fulop[1], Krisztina Kovacs[6], Zsuzsanna Nagy[7], Jason Sparks[1], Attila Miseta[8], Gabriel Mazzucchelli[9], Hitoshi Hashimoto[10] and Attila Bardosi[3]* ID

[1] *Department of Anatomy, MTA-PTE PACAP Research Group, University of Pecs Medical School, Pécs, Hungary*
[2] *Institute of Pathology, University of Heidelberg, Heidelberg, Germany*
[3] *Center for Histology, Cytology and Molecular Diagnostics, Trier, Germany*
[4] *Proteopath GmbH, Trier, Germany*
[5] *Department of Anatomy, Histology and Embryology, Faculty of Medicine, University of Debrecen, Hungary*
[6] *Department of Biochemistry and Medical Chemistry, University of Pecs Medical School, Pécs, Hungary*
[7] *Second Department of Internal Medicine, University of Pecs Medical School, Pécs, Hungary*
[8] *Department of Laboratory Medicine and Szentagothai Research Centre, University of Pecs Medical School, Pécs, Hungary*
[9] *Laboratory of Mass Spectrometry (LSM) — MolSys, Department of Chemistry, University of Liège, Belgium*
[10] *Laboratory of Molecular Neuropharmacology, Graduate School of Pharmaceutical Sciences, Osaka University, Japan*

**Correspondence to: Attila Bardosi, Center for Histology, Cytology and Molecular Diagnostics, Max-Planck-Strasse 5, 54296 Trier, Germany.
E-mail: abardosi@web.de*

Abstract

Dysregulation of neuropeptides may play an important role in aging-induced impairments. Among them, pituitary adenylate cyclase-activating polypeptide (PACAP) is a potent cytoprotective peptide that provides an endogenous control against a variety of tissue-damaging stimuli. We hypothesized that the progressive decline of PACAP throughout life and the well-known general cytoprotective effects of PACAP lead to age-related pathophysiological changes in PACAP deficiency, supported by the increased vulnerability to various stressors of animals partially or totally lacking PACAP. Using young and aging CD1 PACAP knockout (KO) and wild type (WT) mice, we demonstrated pre-senile amyloidosis in young PACAP KO animals and showed that senile amyloidosis appeared accelerated, more generalized, more severe, and affected more individuals. Histopathology showed age-related systemic amyloidosis with mainly kidney, spleen, liver, skin, thyroid, intestinal, tracheal, and esophageal involvement. Mass spectrometry-based proteomic analysis, reconfirmed with immunohistochemistry, revealed that apolipoprotein-AIV was the main amyloid protein in the deposits together with several accompanying proteins. Although the local amyloidogenic protein expression was disturbed in KO animals, no difference was found in laboratory lipid parameters, suggesting a complex pathway leading to increased age-related degeneration with amyloid deposits in the absence of PACAP. In spite of no marked inflammatory histological changes or blood test parameters, we detected a disturbed cytokine profile that possibly creates a pro-inflammatory milieu favoring amyloid deposition. In summary, here we describe accelerated systemic senile amyloidosis in PACAP gene-deficient mice, which might indicate an early aging phenomenon in this mouse strain. Thus, PACAP KO mice could serve as a model of accelerated aging with human relevance.
Copyright © 2018 Pathological Society of Great Britain and Ireland. Published by John Wiley & Sons, Ltd.

Introduction

Previous findings indicate that PACAP progressively declines during aging and its deficiency substantially increases tissue vulnerability [1,2]. Here, we hypothesize that PACAP deficiency leads to age-related systemic degeneration, causing accelerated pre-senile systemic amyloidosis, as a representation of the aging-related chronic condition (physiological as well as disease-related) in mice.

Amyloidosis is a heterogeneous group of diseases, from small local to generalized systemic forms, characterized by the deposition of amyloid fibrils caused

by inappropriate protein aggregation [3–7]. Many forms affect the brain (such as Alzheimer's and Parkinson's disease), while others leave the CNS intact [3,8]. Advances in proteomics have revealed more than 30 different proteins prone to fibril formation in the complex amyloid matrix [6,9–13]. Excessive production, mutations or proteolytic digestion can result in an amyloidogenic protein form, the fibril formation of which requires several factors, such as proteases, nucleating particles, chaperons, matrix molecules, and microenvironment [10,13], the balance of which can be disturbed in aging, when senile amyloidosis occurs in several mouse strains as well as in humans [8].

Natural peptides or peptide-based molecules preventing amyloid formation or its progression have been recognized [3,14] as molecules with possible interference in amyloidogenic mechanisms including stabilizing non-toxic amyloid species, redirecting aggregation pathways, trapping toxic amyloid species or retaining native protein conformation [15]. In turn, dysregulation of neuropeptides may play a role in aging-induced impairments and accelerate the formation of amyloid deposits [16]. PACAP is a highly effective neuro- and general-cytoprotective peptide that provides endogenous control in tissue damage by exerting a unique combination of simultaneous promotion of anti-inflammatory, anti-apoptotic, and antioxidant pathways mainly via PAC1 receptor and VPAC1/2 receptors [1,2,17–21].

PACAP decline has been reported in aging human and monkey brains [22,23] and in aging rat cerebrovascular cells, where decreased release of endothelial PACAP upon oxidative stress can be observed [24,25]. Lack of endogenous PACAP results in a variety of abnormalities [2,18]; for example, a lower level or absence of PACAP leads to increased vulnerability and accelerated aging, as shown in the retina and by the reduced antioxidant capacity of aging KO mice [22,26,27]. These alterations may lead to the reduced life span and increased mortality (approximately twice as high as in WT mice) of mice lacking PACAP, as observed in our PACAP KO colony. In PACAP KO mice, mass spectrometric (MS) analysis uncovered an altered homeostatic protein pattern resulting in disturbed energy balance, the compensation of which is compromised under a challenged environment and possibly during aging [28]. Our main hypothesis is that PACAP deficiency mimics premature aging with pre-senile systemic degenerative changes. Here, we report the results of detailed systemic histopathological analysis showing accelerated systemic amyloidosis in mice lacking PACAP. MS-based proteomic analysis of deposits identified apolipoprotein (apo)-AIV-type (Apo-AIV) amyloidosis with several other amyloidogenic components. All amyloid-associated proteins were further investigated by matrix-assisted laser desorption/ionization (MALDI) imaging MS (IMS) to directly map the distribution of corresponding peptides in tissue.

Materials and methods

Animals

The generation of KO mice on a CD1 background has been described previously [29]. Maintenance, backcrossing for ten generations of the in-house-bred KO mice, and all procedures were performed with permission (BA02/2000-24/2011; BA02/2000-20/2006 [29,30]). WT ($n = 29$) and homozygous PACAP KO mice ($n = 29$) were grouped into 3- to 12- (young) and 13- to 24-month-old (aging) groups. Genotyping from tail samples was performed at sacrifice using a Phire Animal Tissue Direct PCR Kit (Thermo Fisher Scientific, Waltham, MA, USA) [30].

Histological analysis

Mice ($n = 15$ WT, 15 KO) were killed under isoflurane anesthesia (AErrane, Baxter, Budapest, Hungary) and removed organs (see supplementary material, Supplementary materials and methods for a detailed list) were placed in 4% buffered paraformaldehyde and embedded in paraffin wax, and 3-μm-thick sections were cut and stained with hematoxylin and eosin (Paraform Sectionable Cassette System, Tissue-Tek X-Press, AutoTek120 and Prisma Film Coverslipper HQ, smart automation system – Sakura Finetek, Alphen aan den Rijn, The Netherlands). Parallel sections were stained with Congo red, the gold standard for amyloid fibrils [31], which displayed amyloid deposits in red-orange under normal light, whereas apple-green birefringence was indicative of amyloid under polarized light. A semi-quantitative scoring of Congo red-positive deposits from 0 to 3 was performed according to pathological criteria [32,33]: amyloid index 0: no amyloid; 1: slight focal; 2: moderate/severe focal or slight diffuse; 3: massive diffuse amyloid deposit. As no gender differences were observed, scores are presented combined [32]. Percentages of affected individuals for each organ were also evaluated. Statistical comparison between WT and KO mice was made with a non-parametric Mann–Whitney test. For comparison between age groups, the Kruskal–Wallis test and Dunn's multiple comparison test were used.

Laser microdissection (LMD)–based microproteomic analysis

Sections of intestinal villi with massive amyloidosis were chosen for LMD-based microproteomic analysis to characterize the type of amyloidosis. Characterization was performed using a recently developed method for proteomic analysis of small laser-microdissected formalin-fixed, paraffin-embedded (FFPE) samples [34–36]. The procedure for LMD-based microproteomics has been described previously [37] and uses in-solution tryptic digestion of proteins directly from tissue pieces. The released peptides are then separated by reverse-phase liquid chromatography directly bridged to a quadrupole-Orbitrap mass spectrometer

Table 1. Percentage of animals showing signs of amyloidosis

Organ	% of WT 3–12 months	% of WT 13–24 months	% of KO 3–12 months	% of KO 13–24 months
Spleen	0	67	67	100
Esophagus	0	43	71	75
Kidney	0	33	57	86
Liver	0	17	29	100
Thyroid gland	0	25	60	100
Skin	14	67	57	88
Intestines	10	78	56	100
Heart	0	14	25	29
Lung	0	33	50	63
Stomach	0	60	43	50

(see supplementary material, Supplementary materials and methods for details). MaxQuant version 1.5.2.8 was used for raw file analysis.

MALDI IMS

Intestine was selected as it contained abundant deposits in well-circumscribed areas in the villi. Five-micrometer-thick sections were cut from two different FFPE specimens and mounted onto conductive indium tin oxide (ITO)-coated glass slides (Bruker Daltonik, Bremen, Germany).

Sample processing consisted of deparaffinization of the tissue sections, antigen retrieval, on-tissue spraying of trypsin and tissue digestion, and finally matrix deposition (see supplementary material, Supplementary materials and methods for details).

MS measurements were carried out using a rapifleX MALDI Tissuetyper (Bruker Daltonik, Bremen, Germany) instrument at $50\,\mu m$ spatial resolution from m/z 640 to m/z 3000. External calibration was performed using Peptide calibration standard II (Bruker Daltonik). FlexImaging 5.0 (Bruker Daltonik) was used to visualize ion images; all displayed intensities were normalized to total ion count (TIC). Further data analysis was performed with SCiLS Lab 2018b software (SCiLS, Bremen, Germany).

Immunohistochemistry for Apo–AIV and molecular analysis

We performed immunostaining using an anti-Apo-AIV antibody (1:200, catalog number NBP1-06019; Novus Biologicals, Littleton, CO, USA) to confirm the presence of Apo-AIV, the main amyloid component, in tissues with abundant deposits: intestine, kidney, liver, and spleen. Staining was performed using a Ventana Bench-Mark XT Ultra (Ventana Medical Systems, Inc, Tucson, AZ, USA). A method control was performed by omitting the primary antiserum, and which produced no staining. PCR for amyloid protein mRNAs was performed from intestinal samples from aging WT and KO mice ($n = 3$ per group) with confirmed amyloidosis. In addition, kidney homogenates ($n = 4$ per group) were processed for cytokine array analysis (Proteome Profiler Mouse Cytokine Array Kit, Panel A, R&D System, Minneapolis, MN, USA), according to the manufacturer's

instructions. Statistical analysis was performed using two-way ANOVA followed by Fisher's *post hoc* test. The sequences of primer pairs are given in the supplementary material, Table S1 and further details of PCR in the supplementary material, Supplementary materials and methods.

Laboratory analyses of serum and blood

Blood was collected from young and aging WT and KO mice ($n = 7$ per each group) under isoflurane overdose into BD Vacutainer tubes with sodium heparin for serum analysis or EDTA for routine complete blood count (Becton, Dickinson and Company, NJ, USA). Na^+ and K^+ ions, alkaline phosphatase (ALP), creatinine, cholesterol, triglyceride, and high- and low-density lipoprotein (HDL, LDL) were measured with a COBAS 8000 analyzer (Roche Ltd, Rotkreuz, Switzerland), while blood count was measured with a Sysmex XN-1000-V Multispecies Hematology Analyzer (Sysmex Hungaria, Budapest, Hungary). Statistical analysis of serum parameters and blood count was performed using two-way ANOVA followed by Fisher's or Bonferroni's *post hoc* test, respectively.

Results

Histopathological evaluation

Analysis of peripheral organs revealed more diffuse and more severe amyloidosis in the KO animals with progressive aging. First, we analyzed the number of animals with amyloidosis (Table 1). Signs in most organs had already appeared at 6 months in KO mice, whereas deposits appeared in WT animals typically at 15 months. The percentage of animals with deposits was markedly higher in KO groups than in their age-matched WT mates. In WT mice, most severe deposits were observed in organs that showed some amyloidosis already at young ages, such as skin and intestines. In aging KO mice, liver, spleen, intestines, and thyroid gland were positive in all animals. Amyloid distribution in different organs is described below. The distribution of deposits was similar in both groups in general, with differences

in the time of appearance and quantity. Altogether, amyloidosis manifested evidently earlier, progressed more rapidly with a higher degree of severity at older ages, and affected more KO individuals.

Gastrointestinal tract

Esophageal lamina propria contained wide, filamentous, compact deposits in a linear distribution. In the stomach, mostly the interglandular connective tissue and vessels were affected (Figure 1A: A, B). Small intestinal villi showed the highest levels of deposits in the lamina propria and vessel walls, and interglandular connective tissue in small and large intestine was filled in severe cases with aging (Figure 1A: C–F). Salivary glands were unaffected; only occasional perivascular tissues and vessel walls were involved. In the liver, perivascular deposits were around portal vessels and the central vein. In sinusoidal walls, homogeneous amyloid deposits were seen around central veins (Figure 1B: A). Patches of degenerated hepatocytes were observed in KO mice, in contrast to WT mice, where only single cells were affected distal from central veins. Scattered degenerating hepatocytes, closely associated with deposits, were surrounded by amyloid-containing macrophages. Intramural vascular deposits were found in the pancreas in a few animals (Figure 1B: B), and periductal connective tissue septa were affected, but islets, exocrine acini, and the gallbladder were unaffected.

Respiratory tract

In the trachea and larynx, amyloid was deposited in vessel walls. Under the parietal pleura, discrete focal deposits were observed in the lung, and intraparenchymal vessels contained amyloid. Alveolar cells and bronchial respiratory epithelium were unaffected.

Urogenital system

Deposits mainly affected kidney glomeruli; 90% were damaged by the amorphous deposits in severe cases in older KO animals, while amyloid was missing from tubules or interstitium (Figure 1B: C–E). No deposits were found in the uterus, vagina or ovaries of female mice, or in the testis, epididymis or seminal vesicles in males, only in peritesticular venous vessel walls.

Musculoskeletal and cardiovascular systems

In the skeletal muscle, small endomysial vessels were positive using Congo red. Joints or bones were unaffected. In the cardiac muscle, sub-endocardial deposits were occasionally observed. In larger arteries and veins, deposits were mainly present both intramurally and perivascularly.

Immune system and skin

Only a few small patches were observed in WT spleens. Approximately 10% of the spleen was involved, without

affecting the basic structure in young KO mice, while in older mice, approximately 65–70% of the spleen parenchyma was replaced by amyloid deposits in severe cases (Figure 1C: A, B). Deposits were seen in white and red pulps, and the sinusoid wall was infiltrated. Lymph nodes did not display positive deposits; only perinodular vessels contained some amyloid. No deposits were found in the thymus. In the skin, the main location of the deposits was the dermal papillary layer, continuous with the homogeneous mass in the connective tissue surrounding appendages (hair follicles and sebaceous and sweat glands) and vessel walls (Figure 1C: C, D).

Endocrine glands and nervous system

Diffuse deposits were observed surrounding thyroid follicles, which were free of deposits but often atrophic, resulting in fibrotic transformation of the parenchyma (Figure 1C: E, F). Other glands (adrenal, parathyroid, pituitary) displayed no positivity, similarly to the CNS, peripheral nerves, and eye (cornea, choroid layer, retina, sclera).

In several additional organs, perivascular connective tissue displayed some positivity. In addition, brown adipose tissue, typically present in mice in larger amounts, displayed deposits mainly in the connective tissue between adipocytes. In other organs, only sporadic, vessel wall-related amyloid deposits were occasionally observed (Figure 1B: F).

Statistical analysis of the amyloid index revealed a significant overall effect of PACAP in the spleen, esophagus, kidney, liver, thyroid gland, trachea, and skin (Figure 2A). The amyloid index in the young and older age groups also revealed significant differences between WT and KO groups. In most organs, the severity of amyloidosis was similar in aging WT and young KO mice, showing that amyloidosis had already reached senile levels at a young age as a result of a lack of PACAP (Figure 2B). Altogether, these data show that PACAP deficiency accelerates the appearance of senile systemic amyloidosis, resulting in pre-senile degeneration with more generalized and more severe amyloid deposition.

LMD-based microproteomic analysis

LMD-based microproteomic analysis of amyloid deposits allowed confident identification of 13 235 peptides, corresponding to 2172 proteins. Fifteen known amyloidosis-associated proteins were identified [10]. These were, in order of intensity (Figure 3), Apo-AIV, Apo-E, serum amyloid P-component, Apo-AI, Apo-AII, transforming growth factor-beta-induced protein ig-h3, gelsolin, Ig alpha chain C region, Ig kappa chain C region, Ig gamma-1 chain C region, serum amyloid A-1 protein, transthyretin, beta-2-microglobulin, lysozyme C-1, and Ig gamma-3 chain C region (gene names: Apoa4, Apoe, Apcs, Apoa1, Apoa2, Tgfbi, Gsn, Igha, Ighg1, Saa1, Trt, B2m, Lyz1, Ighg3, respectively). The most abundant proteins were Apoa4, Apoe, Apcs, and Apoa1.
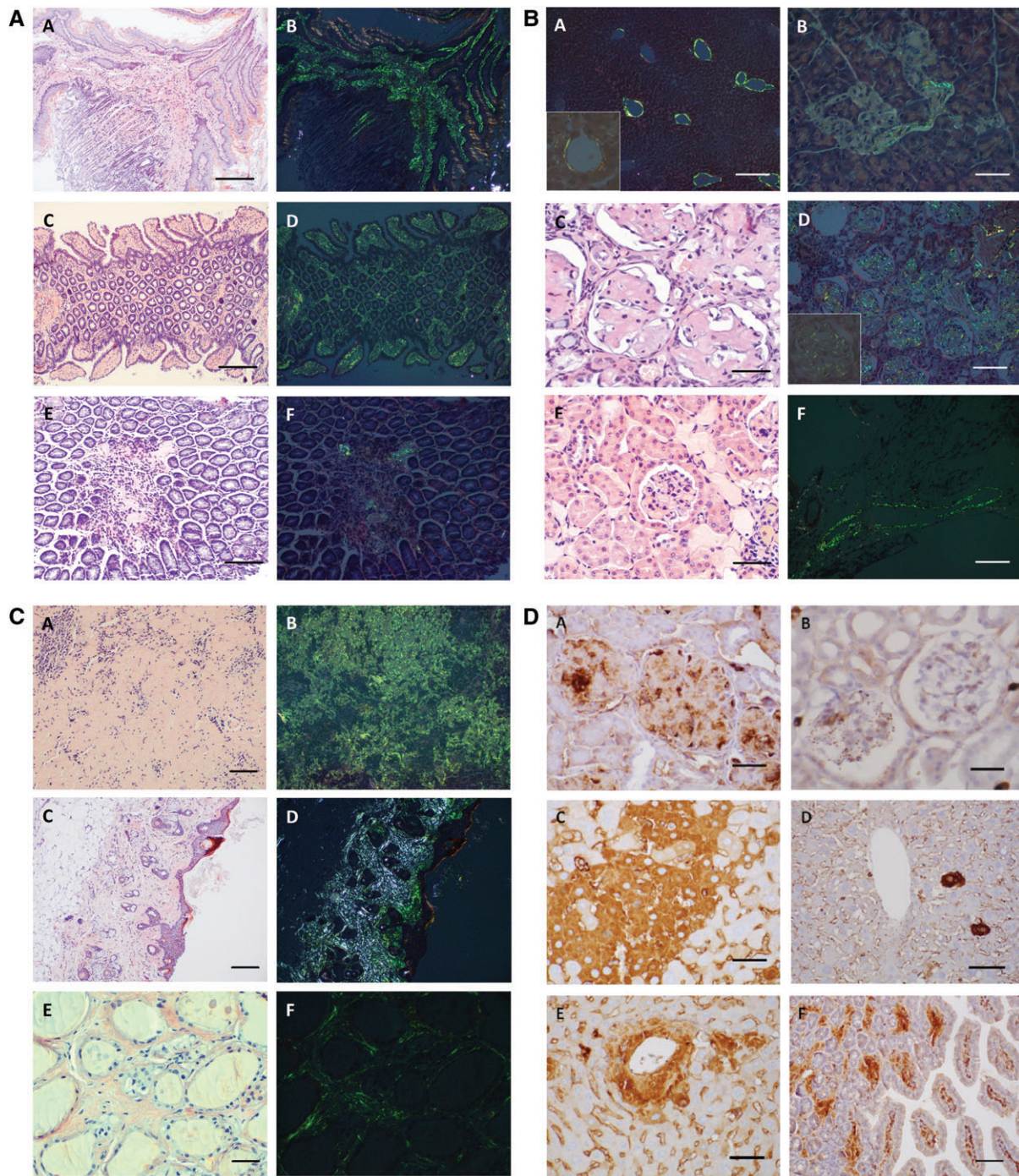
Figure 1. Representative photomicrographs of amyloid deposits in tissues from PACAP KO mice and of Apo-AIV immunoreactivity in aged WT and PACAP KO mice. (Part A) Amyloid deposits in esophagus (A, B) and small intestine of a 16-month-old PACAP KO mouse (C, D), and WT of the same age (E, F). Congo red staining without polarizing light (A, C, E) showing red homogeneous amyloid deposits confirmed in the same locations of the same sections with polarizing light displaying apple-green birefringence (B, D, F). Scale bar = 200 μm (A, B) or 170 μm (C–F). (Part B) Amyloid deposits in liver (A), pancreas (B), kidney (C, D), and a vein in adipose tissue (F) of a 16-month-old PACAP KO mouse and in the kidney of WT of the same age (E). Congo red staining without polarizing light (C, E) showing red homogeneous amyloid deposits, and apple-green birefringence under polarizing light (A, B, D, F). Insets (A, D) show an enlarged area of a central vein in the liver (A) and a renal glomerulus (D). Scale bar = 350 μm (A), 80 μm (B, E), 30 μm (C), 100 μm (D), or 200 μm (F). (Part C) Amyloid deposits in spleen (A, B), skin (C, D), and thyroid gland (E, F) of a 16-month-old PACAP KO mouse. Congo red staining without polarizing light (A, C, E) showing red homogeneous deposits confirmed in the same sections with polarizing light displaying apple-green birefringence (B, D, F). Scale bar = 250 μm (A–D) or 80 μm (E, F). (Part D) Apo-AIV immunoreactivity in kidney glomeruli of aging KO (A) and aging WT (B), in degenerated hepatocytes in patches of an aging KO (C), and in single hepatocytes in an aging WT mouse (D) and around the central vein in an aging KO animal (E). Intestinal villi displaying immunoreactivity in an aging KO mouse (F). Scale bar = 30 μm (A, B), 70 μm (C–E) or 150 μm (F).
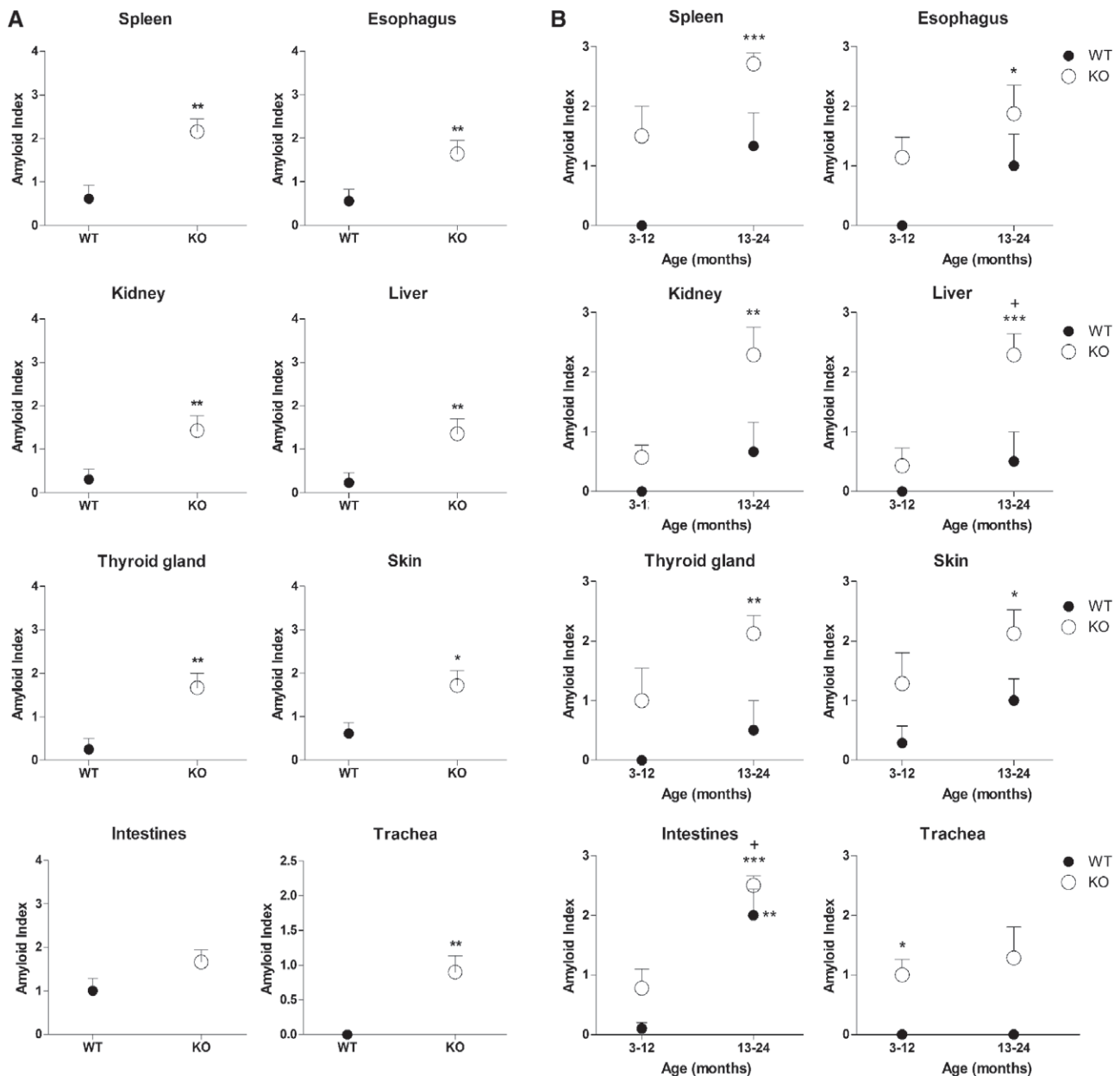
Figure 2. Amyloid index in young and old WT and PACAP KO mice. (A) Overall amyloid index in WT and PACAP KO mice in selected organs with massive amyloid deposits in old age. Mean ±SEM, where *$p < 0.05$ and **$p < 0.01$ versus WT mice. (B) Amyloid index in young (3–12 months) and aging (13–24 months) WT and PACAP KO mice in selected organs with massive amyloid deposits at older ages. Mean ±SEM, where *$p < 0.05$, **$p < 0.01$, and ***$p < 0.001$ versus young WT mice. +$p < 0.05$ versus young PACAP KO mice.

MALDI IMS correlation with LMD-based microproteomic dataset

Sections with Congo red-positive areas were examined under polarized light with digitally marked representative regions superimposed with MALDI data, and spectra profiles were compared between negative and positive areas in order to find discriminant peaks (Figure 4 and supplementary material, Figure S1). Peptide *m/z* values obtained from MALDI MSI were compared with peptides identified by LC–MS/MS to attribute IDs. We found 13 peptides identified by LC–MS/MS matching *m/z* values detected in deposits by MALDI IMS. Seven peptides were assigned to Apoe, four to

Apoa4, one to Apoa1, and one to Apoa2. To evaluate the difference of all *m/z* peptide values through the two regions, the receiver operating characteristic (ROC) test was performed and the area under the ROC curve (AUC) measured was greater than 0.9 for all peptides except for *m/z* 1239.7 and 1743.9, where the AUC was more than 0.7.

Immunohistochemistry for Apo-AIV and molecular analysis

As Apoa4 was identified as the main amyloidosis-related protein in the deposits by LC–MS/MS, we confirmed the presence of this apolipoprotein by
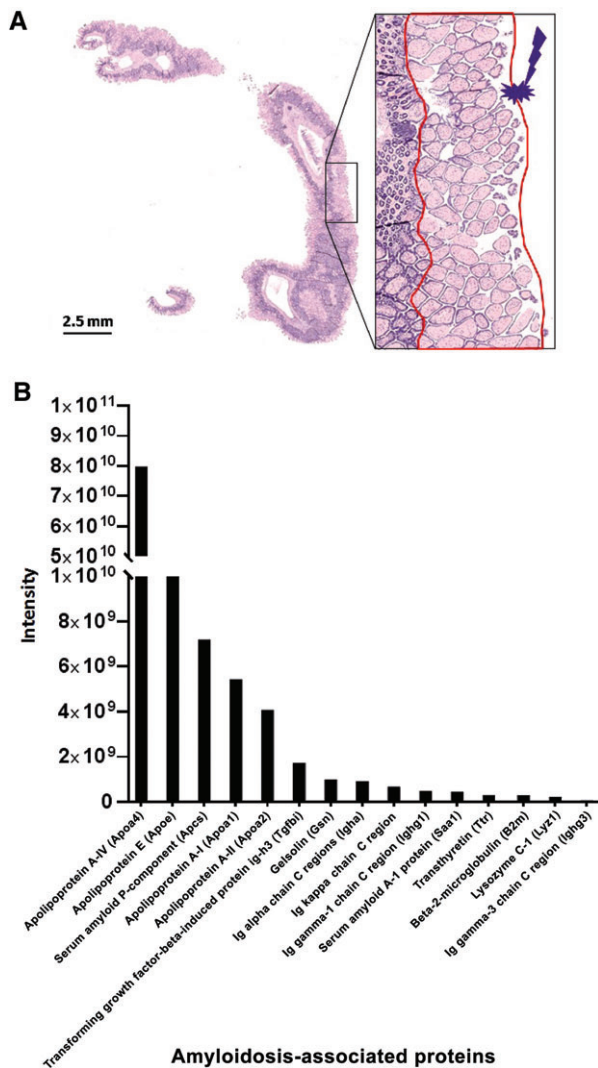
Figure 3. Characterization of the type of amyloidosis using laser microdissection-based microproteomics. (A) Congo red–stained section of the intestine of a PACAP KO mouse. The regions surrounded in red in the inset correspond to the laser-microdissected one from a serial section. (B) Intensities of amyloidosis-related proteins identified in the sample. The high intensity of Apoa4, Apoe, Apcs, and Apoa1 suggests that the amyloidosis type is AApoA4.

immunohistochemistry in the organs where the most massive amyloidosis was found. We found Apo-AIV-positive areas in the examined organs corresponding to the distribution of Congo red-positive regions in aging animals (Figure 1D). In KO mice, Apo-AIV immunopositivity was stronger and more widespread than in WT mice, in accordance with the histopathological observations.

The balance in the expression of mRNA encoding amyloid specific proteins identified with MS in the intestine was disturbed in the absence of PACAP, with some showing stronger, while others weaker expression in the KO samples than in the WT ones (supplementary material, Figure S2). The results of the cytokine array revealed dramatically increased levels of several cytokines in the aging KO samples compared with the other groups. Of those, the most marked changes were observed in BLC (B lymphocyte chemoattractant),

IL-1ra (interleukin-1 receptor antagonist), and RANTES (regulated on activation, normal T-cell expressed and secreted) (Figure 5).

Serum and blood analyses

Serum analysis revealed no difference in Na^+ or K^+ levels. Among the parameters referring to liver and kidney functional deficit, ALP and creatinine were examined, respectively. While there was no difference in ALP levels, serum creatinine levels showed a marked, significant increase in aging versus young PACAP KO mice in contrast to WT animals, where there was no age-related increase. Lipid parameters (HDL, LDL, total cholesterol) showed slight but not statistically significant increases in aging PACAP KO animals (supplementary material, Figure S3). The complete blood count showed no significant alterations between the examined groups.

Discussion

The increased vulnerability to stressors of animals lacking PACAP and its well-known cytoprotective effects support the hypothesis that PACAP deficiency mimics aspects of age-related pathophysiological changes. Here, we have described the premature appearance of severe senile systemic amyloidosis in mice lacking endogenous PACAP. We showed with mass spectrometry-based proteomic analysis, confirmed by immunohistochemistry, that apolipoprotein-AIV was the main amyloid protein in the deposits with several accompanying ones. These findings indicate that in the absence of endogenous PACAP, accelerated age-related degenerative changes occur, pointing to the important role of PACAP in aging-induced systemic processes.

It is still not entirely understood why deposits are formed at an older age and why only in some tissues [38]. Several animal models have been proposed to study age-related systemic amyloidosis, since spontaneous amyloidosis has long been known to occur in various strains of inbred mice [39]. A study in different mice [5] described spontaneous systemic senile amyloidosis in 75% of strains. This was confirmed in a 15-year survey, where a higher incidence of amyloidosis was found in CD1 mice than in others [40]. In our CD1 mice, we found no deposits during the first year in WTs (only in sporadic skin and intestinal spots), but already at early ages in some PACAP KO individuals. Our results, showing a few individuals with slight amyloidosis at 6 months, are also in accordance with the description of spontaneous amyloidosis in aging inbred mice [8]. The observation that the degree of fibril formation showed no gender difference is also in agreement with earlier findings of CD1 and other strains [33,40,41]. Here, we have described a type of age-related systemic amyloidosis with mainly kidney, spleen, liver, skin, thyroid, intestine, stomach, trachea, and esophagus involvement. The severe kidney involvement is also reflected
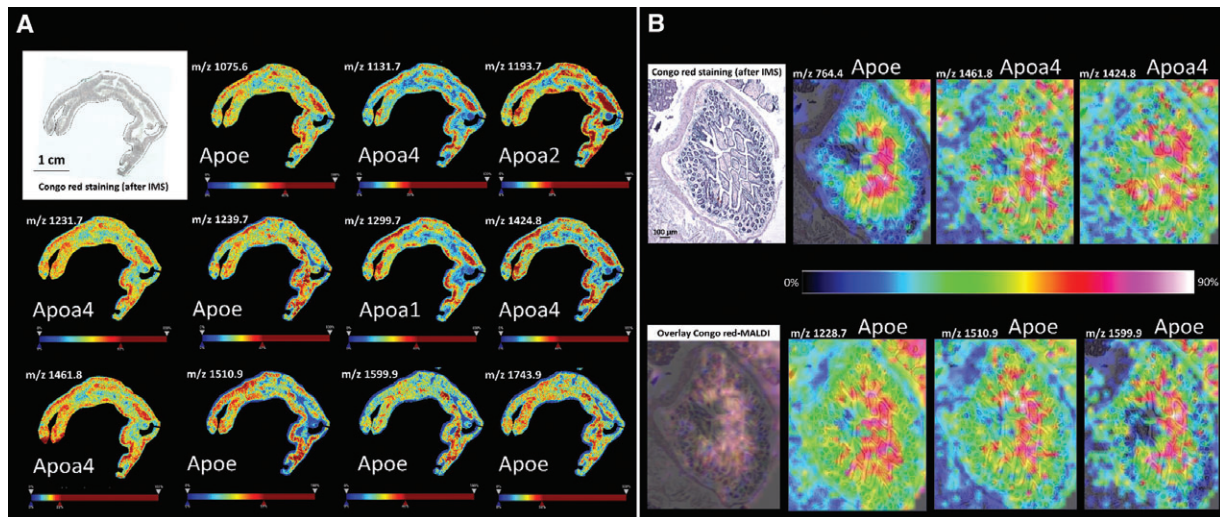
Figure 4. Mass spectrometric imaging of the amyloid deposits. (A) Correlation between Congo red and MALDI images of a mouse intestine tissue sample. MALDI IMS distribution of specific ion peptides identified as Apoe with *m/z* values 1075.6, 1239.7, 1510.9, 1599.9, and 1743.9; Apoa4 with *m/z* values 1131.7, 1231.7, 1424.8, and 1461.8; and Apoa1 with *m/z* value 1299.7 correlates with Congo red positive staining. (B) MALDI IMS distribution of the same ion peptides detected on a different mouse intestine tissue sample. A predictive peptide (*m/z* 764.4) for Apoe protein was also detected correlating exclusively with the amyloid deposits. Overlay of Congo red and MALDI images shows co-localization of the different *m/z* species with extensive overlap with the amyloid deposits. MALDI IMS analysis was performed on the adjacent section to the Congo red staining section. The chromatic scale color bar indicates the relationship between the color of a peak displayed and the peak intensity in arbitrary units, with red and blue indicating the highest and lowest intensity color, respectively.
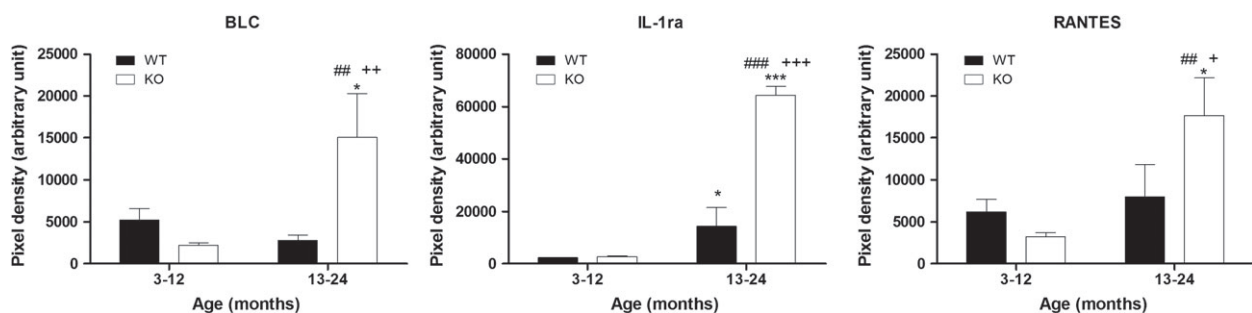

Figure 5. Results from cytokine array analysis. Plots show pixel densities of BLC (B-lymphocyte chemoattractant), IL-1ra (interleukin-1 receptor antagonist), and RANTES (regulated on activation, normal T-cell expressed and secreted) in young and aging wild-type (WT) and PACAP knockout (KO) kidneys. Mean $\pm$SEM. $*p < 0.05$, $***p < 0.001$ versus WT 3–12; $^{\#\#}p < 0.01$, $^{\#\#\#}p < 0.001$ versus KO 3–12; $^+p < 0.05$, $^{++}p < 0.01$, $^{+++}p < 0.001$ versus WT 13–24.

in higher creatinine levels, indicating functional disturbance. While most forms of systemic amyloidosis affect joints and periarticular tissues [42], we did not observe articular amyloid deposits. Our observation that the CNS and peripheral nerves lacked deposits is in accord with earlier findings in systemic amyloidosis [8,43,44].

It is now known that amyloid deposits contain several distinct main and accompanying minor components [10,45] that can be structurally unrelated and can be deposited in different locations in conglomerates or in distinct foci [46,47]. Proteomic approaches have identified the composition of the deposits [5,48–53], with Apoe, serum amyloid P component, Apoa4, and Apoa1 present in almost all amyloidosis types as incorporated proteins [10]. Of these, the first three are considered specific amyloidosis biomarkers. We used LC–MS/MS-based proteomics, adequate for the identification of amyloidosis-associated proteins and the subsequent classification of amyloidosis

subtypes [10,34–36,48,52,54,55]. In the present context, deposits could be found in large quantities within different organs. We could identify with high confidence 15 amyloidosis-related proteins, with Apoa4 having the highest abundance [10,48]. It is noteworthy that non-amyloidosis-associated proteins reported in human cases of AApoAIV amyloidosis such as vitronectin, serum albumin, clusterin, collagen alpha-2 (I) chain, collagen alpha-1 (I) chain, and actin [48] were also found in our samples. The combined analysis of LMD-based microproteomic and MALDI IMS resulted in a more comprehensive characterization, similarly to previous descriptions in renal biopsies [56]. By matching the peptide masses identified by LC–MS/MS with MALDI IMS, 13 peptides related to Apoa4 ($n_{peptides} = 4$), Apoe ($n_{peptides} = 7$), Apoa1 ($n_{peptides} = 1$), and Apoa2 ($n_{peptides} = 1$) were detected exclusively in amyloid regions, in excellent concordance with the Congo red-positive areas.

The systemic amyloidosis-associated protein described here was predominantly Apo-AIV, confirmed by Apo-AIV immunohistochemistry. We could also detect mRNA for the proteins identified by MS in the same tissues, but the balance of the different amyloidogenic protein mRNAs was disturbed, possibly indicating a pathological feedback for production due to the local deposits and/or disturbed synthesis. Apolipoproteins play a role in lipid metabolism and transport [57] with susceptibility to form fibrils, possibly due to their intrinsic flexibility [46]. Considering the role of apolipoproteins in lipid metabolism, we ran a laboratory test for the main lipid parameters, but found no significant differences. This indicates no major disturbances in lipid metabolism in general, but raises the possibility of some other mechanisms leading to apolipoprotein deposits in KO tissues. Apolipoproteins have long been associated with fibril formation in cerebral and systemic amyloidosis [58]. Among apolipoproteins, Apo-AIV shows age-related decline (which we could also detect in KO mice) and has the highest sensitivity to denaturation and vulnerability to environmental disturbances [46]. Recent reports using proteomics-based assays have shown a more widespread occurrence of AApoAIV amyloidosis than previously thought [48,50]. Apo-E can also be consistently detected in deposits [59,60], and Apo-AI has long been associated with systemic amyloidosis with different localizations [51,61]. AApoAIV- and AApoE-dominating systemic amyloidosis is known in inbred foxes with mainly kidney, spleen, oral cavity, and vascular involvement [62]. Apo-AII is also known to form senile fibrils [33,44,63] including inbred mouse strains [8]. Serum amyloid P component, a constituent in all amyloid deposits [10,63,64], was also found in our samples. Although its role is controversial, i.e. both anti-amyloidogenic and pro-amyloidogenic effects have been described [65], its presence is usually attributed to its role in stabilizing the fibrils, thereby preventing proteolytic degradation [66,67]. A recent study has suggested that in addition to the most common proteins, serum amyloid P component, Apo-E, and Apo-AIV, the amyloid proteomic signature should also include vitronectin and clusterin as co-deposited proteins [53]. We could also detect other proteins associated with amyloid formation, such as gelsolin, transthyretin, Ig kappa and gamma-1 chain C region, serum amyloid A1, beta2 microglobulin, and lysozyme C1. As these proteins were detected with relatively low intensities, they do not seem to be major amyloid constituents in PACAP KO mice.

Good animal models are important in studying diseases of protein misfolding, as it is still unknown why the same protein becomes fibrillogenic with age and why only in some tissues [38]. It has been assumed that age-related forms of amyloidosis reflect chronic inflammatory states, high concentrations of amyloidogenic proteins, and a long latent period of seed formation. In our study, chronic inflammation is excluded, due to a lack of histological signs of generalized inflammation or changes in blood cell counts. However, we detected an altered cytokine profile, especially in aging KO mice. These data indicate a disturbed balance of pro- and anti-inflammatory cytokines and may lead to a shift in the cytokine profile towards a pro-inflammatory milieu, possibly creating a more favorable microenvironment for amyloid deposition in mice lacking PACAP. However, the altered cytokine profile might as well be the consequence of amyloid deposition, leading to upregulation of both pro- and anti-inflammatory cytokines. Earlier studies found differences in the proteome of PACAP KO mice, also leading to a disturbed energy balance, which is possibly further disturbed in aging [28]. Alterations in cytokine expression have been described earlier in several experimental paradigms after PACAP treatment and have been suggested as an aggravating factor in slower regeneration capacity of KO mice [68,69].

Age-related degenerative diseases are increasing, and the problem goes far beyond the two best-known diseases, Alzheimer's and Parkinson's, with protein misfolding in the background [70]. PACAP levels decline with age in humans and experimental animals [71], as shown in rhesus monkey and post-mortem human brains of Alzheimer's patients and in cognitive decline preceding the disease [22,23,72,73], with an association between PACAP levels and disease scores. The few data available to date indicate that PACAP deficiency accelerates aging. Aging KO animals display higher levels of oxidative stress [26], an earlier appearance of retinal degeneration [27], and decreased tear secretion with increased corneal keratinization [74]. In the present study, we have described accelerated systemic senile amyloidosis in PACAP-deficient mice, which might indicate an early aging phenomenon in this strain. Thus, PACAP KO mice could serve as a model of accelerated aging with human relevance, similarly to the widely used senescence-accelerated mouse, which also displays spontaneous age-associated amyloidosis [41,74,75]. Exogenous PACAP can compensate the lack of PACAP, as shown in several acute injury models in KO mice. Among others, PACAP administration could reduce the toxic effects of ethanol or oxidative stress in cerebellar neurons isolated from PACAP KO mice [76]. Exogenous PACAP addition could also attenuate the increased ischemia-induced lesions in KO retinas [77]. Furthermore, Ohtaki *et al* found a greater infarct volume and worse behavioral deficits in hetero- and homozygous PACAP-deficient mice than in WT ones. However, both infarct volume and neurological deficit scores were improved by PACAP injection [69]. The effectivity of factors slowing down misfolded fibril formation and their aggregation decreases, while amyloidogenic mechanisms are accelerated with aging, especially in cases of genetic susceptibility [70,78,79]. Alterations in metabolic enzymes might partially account for the decreased antioxidant and detoxifying capacity of PACAP KO mice [2,28]. The disturbed balance in homeostatic molecules, inflammatory factors, and metabolic enzymes may be compensated at a young age under normal conditions, while they create an unfavorable
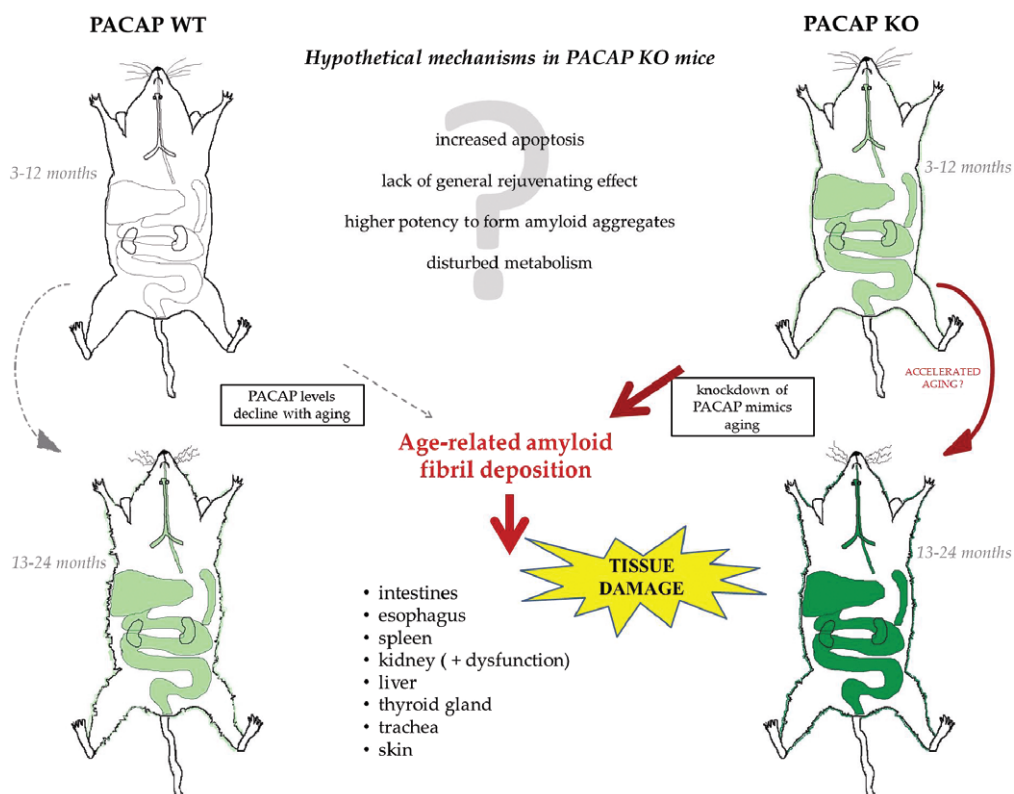
Figure 6. Graphical summary of the main findings showing that lack of PACAP accelerates and aggravates the appearance of senile systemic amyloidosis. Green color indicates the appearance of amyloid deposits. Only organs with deposits are depicted, with darker colors indicating more severe amyloidosis.

milieu for increased vulnerability in cases of injury and aging-related processes. Several other properties of PACAP might be involved in cytoprotection in amyloidosis; for example, PACAP prevents toxic amyloid-beta formation [80,81], rescues cells from amyloid toxicity [73,82], acts against increased apoptosis associated with amyloidosis [83,84], and has a unique potency to bind to negatively charged glycosaminoglycans [85,86], which in turn co-accumulate with amyloid [87]. It is proposed that PACAP plays a role in the complex cellular interactions that lead to tissue destruction in amyloidosis [88] and that the lack of the general rejuvenating effect of PACAP accelerates amyloid formation (Figure 6). PACAP-deficient mice, with their higher vulnerability to noxious stimuli, resemble aging cells with vulnerability to cell death [70]. The physiological or pathological decline of PACAP leads to an increased susceptibility for degenerative processes in the elderly, and thus to accelerated age-related diseases. Our observations point to a multifaceted role of PACAP in aging and age-related degenerative processes and could initiate further studies on the role of PACAP in aging.

Acknowledgements

Author contributions statement

DR, AJ, AT, and ZN prepared tissues. DR, AB, SB, JK, and MK performed histopathological analysis. AJ, AT, and JS performed statistical analysis of the histological scores. RL, RC, JK, and GM performed mass spectrometry analysis. HH provided the gene-deficient animals.

BDF maintained the gene-deficient animal colony and performed PCR genotyping. KK, AJ, and JS performed cytokine array and western blot measurements. AM, AJ, and JS performed laboratory tests of serum samples; TJ performed PCR analysis. DR and AB conceptualized the experiments. DR, AB, AJ, RC, RL, and AT prepared the manuscript.

References

1. Reglodi D, Kiss P, Lubics A, *et al.* Review on the protective effects of PACAP in models of neurodegenerative diseases *in vitro* and *in vivo. Curr Pharm Des* 2011; **17:** 962–972.

2. Reglodi D, Kiss P, Szabadfi K, *et al.* PACAP is an endogenous protective factor – insights from PACAP-deficient mice. *J Mol Neurosci* 2012; **48:** 482–492.

3. Aguzzi A, O'Connor T. Protein aggregation diseases: pathogenicity and therapeutic perspectives. *Nat Rev Drug Discov* 2010; **9:** 237–248.

4. Buxbaum JN, Linke RP. A molecular history of the amyloidoses. *J Mol Biol* 2012; **421:** 142–159.

5. Lavatelli F, Perlman DH, Spencer B, *et al.* Amyloidogenic and associated proteins in systemic amyloidosis proteome of adipose tissue. *Mol Cell Proteomics* 2008; **7:** 1570–1583.

6. Chiti F, Dobson CM. Protein misfolding, amyloid formation, and human disease: a summary of progress over the last decade. *Annu Rev Biochem* 2017; **86:** 27–68.

7. Falk RH, Comenzo RL, Skinner M. The systemic amyloidoses. *N Engl J Med* 1997; **337:** 898–909.

8. Higuchi K, Naiki H, Kitagawa K, *et al.* Mouse senile amyloidosis. ASSAM amyloidosis in mice presents universally as a systemic age-associated amyloidosis. *Virchows Arch B Cell Pathol Incl Mol Pathol* 1991; **60:** 231–238.

9. Cui D, Hoshii Y, Takahashi M, *et al.* An immunohistochemical study of amyloid P component, apolipoprotein E and ubiquitin in human and murine amyloidoses. *Pathol Int* 1998; **48:** 362–367.

10. Dogan A. Amyloidosis: insights from proteomics. *Annu Rev Pathol* 2017; **12:** 277–304.

11. Noda S, So M, Adachi M, *et al.* Thioflavin T-silent denaturation intermediates support the main-chain-dominated architecture of amyloid fibrils. *Biochemistry* 2016; **55:** 3937–3948.

12. Martin EB, Williams A, Richey T, *et al.* Comparative evaluation of p5 + 14 with SAP and peptide p5 by dual-energy SPECT imaging of mice with AA amyloidosis. *Sci Rep* 2016; **6:** 22695.

13. Kisilevsky R, Fraser PE. A beta amyloidogenesis: unique, or variation on a systemic theme? *Crit Rev Biochem Mol Biol* 1997; **32:** 361–404.

14. Fosgerau K, Hoffmann T. Peptide therapeutics: current status and future directions. *Drug Discov Today* 2015; **20:** 122–128.

15. Brahmachari S, Paul A, Segal D, *et al.* Inhibition of amyloid oligomerization into different supramolecular architectures by small molecules: mechanistic insights and design rules. *Future Med Chem* 2017; **9:** 797–810.

16. Ogren SO, Kuteeva E, Elvander-Tottie E, *et al.* Neuropeptides in learning and memory processes with focus on galanin. *Eur J Pharmacol* 2010; **626:** 9–17.

17. Somogyvari-Vigh A, Reglodi D. Pituitary adenylate cyclase activating polypeptide: a potential neuroprotective peptide. *Curr Pharm Des* 2004; **10:** 2861–2889.

18. Vaudry D, Falluel-Morel A, Bourgault S, *et al.* Pituitary adenylate cyclase-activating polypeptide and its receptors: 20 years after the discovery. *Pharmacol Rev* 2009; **61:** 283–357.

19. Reglodi D, Tamas A (Eds). *Pituitary Adenylate Cyclase Activating Polypeptide – PACAP. Current Topics in Neurotoxicity*, Vol 11. Springer Nature: New York, 2016.

20. Abad C, Waschek JA. Immunomodulatory roles of VIP and PACAP in models of multiple sclerosis. *Curr Pharm Des* 2011; **17:** 1025–1035.

21. Seaborn T, Masmoudi-Kouli O, Fournier A, *et al.* Protective effects of pituitary adenylate cyclase-activating polypeptide (PACAP) against apoptosis. *Curr Pharm Des* 2011; **17:** 204–214.

22. Han P, Caselli RJ, Baxter L, *et al.* Association of pituitary adenylate cyclase-activating polypeptide with cognitive decline in mild cognitive impairment due to Alzheimer disease. *JAMA Neurol* 2015; **72:** 333–339.

23. Han P, Nielsen M, Song M, *et al.* The impact of aging on brain pituitary adenylate cyclase activating polypeptide, pathology and cognition in mice and rhesus macaques. *Front Aging Neurosci* 2017; **9:** 180.

24. Banki E, Sosnowska D, Tucsek Z, *et al.* Age-related decline of autocrine pituitary adenylate cyclase-activating polypeptide impairs angiogenic capacity of rat cerebromicrovascular endothelial cells. *J Gerontol A Biol Sci Med Sci* 2015; **70:** 665–674.

25. Tripathy D, Sanchez A, Yin X, *et al.* Age-related decrease in cerebrovascular-derived neuroprotective proteins: effect of acetaminophen. *Microvasc Res* 2012; **84:** 278–285.

26. Ohtaki H, Satoh A, Nakamachi T, *et al.* Regulation of oxidative stress by pituitary adenylate cyclase-activating polypeptide (PACAP) mediated by PACAP receptor. *J Mol Neurosci* 2010; **42:** 397–403.

27. Kovacs-Valasek A, Szabadfi K, Denes V, *et al.* Accelerated retinal aging in PACAP knock-out mice. *Neuroscience* 2017; **348:** 1–10.

28. Maasz G, Pirger Z, Reglodi D, *et al.* Comparative protein composition of the brains of PACAP-deficient mice using mass spectrometry-based proteomic analysis. *J Mol Neurosci* 2014; **54:** 310–319.

29. Hashimoto H, Shintani N, Tanaka K, *et al.* Altered psychomotor behaviors in mice lacking pituitary adenylate cyclase-activating polypeptide (PACAP). *Proc Natl Acad Sci U S A* 2001; **98:** 13355–13360.

30. Farkas J, Kovacs L, Gaspar L, *et al.* Construct and face validity of a new model for the three-hit theory of depression using PACAP mutant mice on CD1 background. *Neuroscience* 2017; **354:** 11–29.

31. Linke RP. Highly sensitive diagnosis of amyloid and various amyloid syndromes using Congo red fluorescence. *Virchows Arch* 2000; **436:** 439–448.

32. Seymour JF, Lieschke GJ, Grail D, *et al.* Mice lacking both granulocyte colony-stimulating factor (CSF) and granulocyte-macrophage CSF have impaired reproductive capacity, perturbed neonatal granulopoiesis, lung disease, amyloidosis, and reduced long-term survival. *Blood* 1997; **90:** 3037–3049.

33. Li L, Sawashita J, Ding X, *et al.* Caloric restriction reduces the systemic progression of mouse AApoAII amyloidosis. *PLoS One* 2017; **12:** e0172402.

34. Longuespee R, Alberts D, Pottier C, *et al.* A laser microdissection-based workflow for FFPE tissue microproteomics: important considerations for small sample processing. *Methods* 2016; **104:** 154–162.

35. Herfs M, Longuespee R, Quick CM, *et al.* Proteomic signatures reveal a dualistic and clinically relevant classification of anal canal carcinoma. *J Pathol* 2017; **241:** 522–533.

36. Longuespée R, Casadonte R, Kriegsmann M, *et al.* Proteomic investigation of human cystic echinococcosis in the liver. *Mol Biochem Parasitol* 2017; **211:** 9–14.

37. Longuespee R, Baiwir D, Mazzucchelli G, *et al.* Laser microdissection-based microproteomics of formalin-fixed and paraffin-embedded (FFPE) tissues. *Methods Mol Biol* 2018; **1723:** 19–31.

38. Buxbaum JN. Animal models of human amyloidoses: are transgenic mice worth the time and trouble? *FEBS Lett* 2009; **583:** 2663–2673.

39. Higuchi K, Matsumura A, Honma A, *et al.* Systemic senile amyloid in senescence-accelerated mice. A unique fibril protein demonstrated

in tissues from various organs by the unlabeled immunoperoxidase method. *Lab Invest* 1983; **48:** 231–240.

40. Majeed SK. Survey on spontaneous systemic amyloidosis in aging mice. *Arzneimittelforschung* 1993; **43:** 170–178.

41. Takeshita S, Hosokawa M, Irino M, *et al.* Spontaneous age-associated amyloidosis in senescence-accelerated mouse (SAM). *Mech Ageing Dev* 1982; **20:** 13–23.

42. Perfetto F, Moggi-Pignone A, Livi R, *et al.* Systemic amyloidosis: a challenge for the rheumatologist. *Nat Rev Rheumatol* 2010; **6:** 417–429.

43. Brayton C, Fox JG, Barthold SW, *et al.* Spontaneous diseases in commonly used mouse strains. In *The Mouse in Biomedical Research*. Academic Press, New York, USA, 2006; 623–717.

44. Wang Y, Sawashita J, Qian J, *et al.* ApoA-I deficiency in mice is associated with redistribution of apoA-II and aggravated AApoAII amyloidosis. *J Lipid Res* 2011; **52:** 1461–1470.

45. Woldemeskel M. A concise review of amyloidosis in animals. *Vet Med Int* 2012; **2012:** 427296.

46. Bergstrom J, Murphy CL, Weiss DT, *et al.* Two different types of amyloid deposits – apolipoprotein A-IV and transthyretin – in a patient with systemic amyloidosis. *Lab Invest* 2004; **84:** 981–988.

47. Tashiro F, Yi S, Wakasugi S, *et al.* Role of serum amyloid P component for systemic amyloidosis in transgenic mice carrying human mutant transthyretin gene. *Gerontology* 1991; **37**(suppl 1): 56–62.

48. Dasari S, Amin MS, Kurtin PJ, *et al.* Clinical, biopsy, and mass spectrometry characteristics of renal apolipoprotein A-IV amyloidosis. *Kidney Int* 2016; **90:** 658–664.

49. Brambilla F, Lavatelli F, Di Silvestre D, *et al.* Reliable typing of systemic amyloidoses through proteomic analysis of subcutaneous adipose tissue. *Blood* 2012; **119:** 1844–1847.

50. Obici L, Nuvolone M, Merlini G. Expanding the spectrum of systemic amyloid diseases: a new hint from the kidney. *Kidney Int* 2016; **90:** 479–481.

51. Solomon A, Murphy CL, Kestler D, *et al.* Amyloid contained in the knee joint meniscus is formed from apolipoprotein A-I. *Arthritis Rheum* 2006; **54:** 3545–3550.

52. Vrana JA, Gamez JD, Madden BJ, *et al.* Classification of amyloidosis by laser microdissection and mass spectrometry-based proteomic analysis in clinical biopsy specimens. *Blood* 2009; **114:** 4957–4959.

53. Mollee P, Boros S, Loo D, *et al.* Implementation and evaluation of amyloidosis subtyping by laser-capture microdissection and tandem mass spectrometry. *Clin Proteomics* 2016; **13:** 30.

54. Sethi S, Theis JD, Leung N, *et al.* Mass spectrometry-based proteomic diagnosis of renal immunoglobulin heavy chain amyloidosis. *Clin J Am Soc Nephrol* 2010; **5:** 2180–2187.

55. Sethi S, Vrana JA, Theis JD, *et al.* Laser microdissection and mass spectrometry-based proteomics aids the diagnosis and typing of renal amyloidosis. *Kidney Int* 2012; **82:** 226–234.

56. Casadonte R, Kriegsmann M, Deininger SO, *et al.* Imaging mass spectrometry analysis of renal amyloidosis biopsies reveals protein co-localization with amyloid deposits. *Anal Bioanal Chem* 2015; **407:** 5323–5331.

57. Kohan AB, Wang F, Lo CM, *et al.* ApoA-IV: current and emerging roles in intestinal lipid metabolism, glucose homeostasis, and satiety. *Am J Physiol Gastrointest Liver Physiol* 2015; **308:** G472–G481.

58. Kindy MS, Rader DJ. Reduction in amyloid A amyloid formation in apolipoprotein-E-deficient mice. *Am J Pathol* 1998; **152:** 1387–1395.

59. Kindy MS, King AR, Perry G, *et al.* Association of apolipoprotein E with murine amyloid A protein amyloid. *Lab Invest* 1995; **73:** 469–475.

60. Yamada T, Someya T, Fujita S. Immunotargeting of apolipoprotein E in amyloid: an initial trial in mice. *Ann Clin Lab Sci* 2009; **39:** 134–137.

61. Arciello A, Piccoli R, Monti DM. Apolipoprotein A-I: the dual face of a protein. *FEBS Lett* 2016; **590:** 4171–4179.

62. Gaffney PM, Imai DM, Clifford DL, *et al.* Proteomic analysis of highly prevalent amyloid A amyloidosis endemic to endangered island foxes. *PLoS One* 2014; **9:** e113765.

63. Qian J, Yan J, Ge F, *et al.* Mouse senile amyloid fibrils deposited in skeletal muscle exhibit amyloidosis-enhancing activity. *PLoS Pathog* 2010; **6:** e1000914.

64. Usui I, Kawano H, Ito S, *et al.* Homozygous serum amyloid P component-deficiency does not enhance regression of AA amyloid deposits. *Amyloid* 2001; **8:** 101–104.

65. Ozawa D, Nomura R, Mangione PP, *et al.* Antiamyloidogenic and proamyloidogenic chaperone effects of C-reactive protein and serum amyloid P component. *Amyloid* 2017; **24:** 28–29.

66. Botto M, Hawkins PN, Bickerstaff MC, *et al.* Amyloid deposition is delayed in mice with targeted deletion of the serum amyloid P component gene. *Nat Med* 1997; **3:** 855–859.

67. Togashi S, Lim SK, Kawano H, *et al.* Serum amyloid P component enhances induction of murine amyloidosis. *Lab Invest* 1997; **77:** 525–531.

68. Watson MB, Nobuta H, Abad C, *et al.* PACAP deficiency sensitizes nigrostriatal dopaminergic neurons to paraquat-induced damage and modulates central and peripheral inflammatory activation in mice. *Neuroscience* 2013; **240:** 277–286.

69. Ohtaki H, Nakamachi T, Dohi K, *et al.* Pituitary adenylate cyclase-activating polypeptide (PACAP) decreases ischemic neuronal cell death in association with IL-6. *Proc Natl Acad Sci U S A* 2006; **103:** 7488–7493.

70. Stroo E, Koopman M, Nollen EA, *et al.* Cellular regulation of amyloid formation in aging and disease. *Front Neurosci* 2017; **11:** 64.

71. Reglodi D, Helyes Z, Nemeth J, *et al.* PACAP as a potential biomarker – alterations of PACAP levels in human physiological and pathological conditions. In *Pituitary Adenylate Cyclase Activating Polypeptide – PACAP. Current Topics in Neurotoxicity*, Reglodi D, Tamas A (eds), Vol **11**. Springer Nature: New York, 2016; Ch 48, 815–832.

72. Han P, Liang W, Baxter LC, *et al.* Pituitary adenylate cyclase-activating polypeptide is reduced in Alzheimer disease. *Neurology* 2014; **82:** 1724–1728.

73. Han P, Tang Z, Yin J, *et al.* Pituitary adenylate cyclase-activating polypeptide protects against β-amyloid toxicity. *Neurobiol Aging* 2014; **35:** 2064–2071.

74. Nakamachi T, Ohtaki H, Seki T, *et al.* PACAP suppresses dry eye signs by stimulating tear secretion. *Nat Commun* 2016; **7:** 12034.

75. Takeda T, Matsushita T, Kurozumi M, *et al.* Pathobiology of the senescence-accelerated mouse (SAM). *Exp Gerontol* 1997; **32:** 117–127.

76. Vaudry D, Hamelink C, Damadzic R, *et al.* Endogenous PACAP acts as a stress response peptide to protect cerebellar neurons from ethanol or oxidative insult. *Peptides* 2005; **26:** 2518–2524.

77. Szabadfi K, Atlasz T, Kiss P, *et al.* Mice deficient in pituitary adenylate cyclase activating polypeptide (PACAP) are more susceptible to retinal ischemic injury *in vivo*. *Neurotox Res* 2012; **21:** 41–48.

78. Sukhanova A, Poly S, Shemetov A, *et al.* Implications of protein structure instability: from physiological to pathological secondary structure. *Biopolymers* 2012; **97:** 577–588.

79. Teng MH, Yin JY, Vidal R, *et al.* Amyloid and nonfibrillar deposits in mice transgenic for wild-type human transthyretin: a possible model for senile systemic amyloidosis. *Lab Invest* 2001; **81:** 385–396.

80. Kojro E, Postina R, Buro C, *et al.* The neuropeptide PACAP promotes the alpha-secretase pathway for processing the Alzheimer amyloid precursor protein. *FASEB J* 2006; **20:** 512–514.

81. Postina R. Activation of α-secretase cleavage. *J Neurochem* 2012; **120**(suppl 1): 46–54.

82. Onoue S, Endo K, Ohshima K, *et al.* The neuropeptide PACAP attenuates beta-amyloid (1-42)-induced toxicity in PC12 cells. *Peptides* 2002; **23:** 1471–1478.

83. Chang YT, Wong CK, Chow KC, *et al.* Apoptosis in primary cutaneous amyloidosis. *Br J Dermatol* 1999; **140:** 210–215.

84. Potter KJ, Scrocchi LA, Warnock GL, *et al.* Amyloid inhibitors enhance survival of cultured human islets. *Biochim Biophys Acta* 2009; **1790:** 566–574.

85. Neree AT, Nguyen PT, Bourgault S. Cell-penetrating ability of peptide hormones: key role of glycosaminoglycans clustering. *Int J Mol Sci* 2015; **16:** 27391–27400.

86. Chatenet D, Fournier A, Bourgault S. PACAP-derived carriers: mechanisms and applications. In *Pituitary Adenylate Cyclase Activating Polypeptide – PACAP. Current Topics in Neurotoxicity*, Reglodi D, Tamas A (eds), Vol **11**. Springer Nature: New York, 2016; Ch 9, 133–148.

87. Nishitsuji K, Uchimura K. Sulfated glycosaminoglycans in protein aggregation diseases. *Glycoconj J* 2017; **34:** 453–466.

88. Marin-Argany M, Lin Y, Misra P, *et al.* Cell damage in light chain amyloidosis: fibril internalization, toxicity and cell-mediated seeding. *J Biol Chem* 2016; **291:** 19813–19825.

SUPPLEMENTARY MATERIAL ONLINE

Supplementary materials and methods

Figure S1. Correlation between Congo red and the MALDI image of *m/z* 1228.7 from the mouse intestine tissue section presented in Figure 4

Figure S2. Representative data of three independent RT-PCR reactions of amyloid specific protein mRNAs identified with mass spectrometry of aging WT and KO mice

Figure S3. Main laboratory serum parameters in young and old WT and PACAP KO mice

Table S1. Nucleotide sequences, amplification sites, GenBank accession numbers, amplimer sizes, and PCR reaction conditions for each mouse primer pair are shown